VLF Hiss and Related Plasma Observations in the Polar Magnetosphere

D. A. GURNETT AND L. A. FRANK

Department of Physics and Astronomy
University of Iowa, Iowa City 52240

This paper presents a study of auroral-zone VLF hiss and low-energy charged-particle observations with the Injun 5 satellite. The results of this study provide a direct verification of the association between auroral-zone VLF hiss and intense fluxes, 10^4 to 10^7 electrons $(cm^2\ sec\ ster\ ev)^{-1}$, of low-energy electrons with energies on the order of 100 ev to several kev. On the dayside of the magnetosphere, these low-energy electrons are identified with the dayside polar-cusp region observed at higher latitudes with the Imp 5 satellite. At other local times, through the dawn and dusk regions and into the nightside of the magnetosphere, the VLF hiss and low-energy electron precipitation regions are believed to correspond to the extension of the dayside polar cusp into the distant plasma sheet and downstream magnetosheath on the nightside of the magnetosphere. Intense fluxes of upgoing electrons are often observed in a narrow latitudinal band near the low-energy electron precipitation bands. These upgoing electrons are believed to be associated with another type of VLF emission called a saucer, which is frequently observed with Injun 5. On the basis of present models, the observed VLF hiss intensities cannot be accounted for by incoherent Cerenkov radiation from the observed electron fluxes, thus indicating that a coherent plasma instability mechanism is involved in some, if not all, of the VLF hiss generation. A model for the generation regions of VLF hiss and saucer emissions is discussed.

Intense broad-band VLF and LF radio noise emissions called 'VLF hiss' or 'auroral hiss' are commonly observed at high latitudes with both ground and satellite instrumentation [i.e., *Helliwell*, 1965; *Gurnett*, 1966; *McEwen and Barrington*, 1967; *Laaspere et al.*, 1971]. The frequency spectrum of these VLF hiss emissions is often very broad, extending in some instances from less than 1 to greater than 500 kHz. The maximum power spectral densities of auroral hiss are on the order of 10^{-14} to 10^{-12} watt $(m^2\ Hz)^{-1}$ [*Gurnett*, 1966; *Jørgensen*, 1968]. Since VLF hiss cannot propagate in the whistler mode at frequencies greater than the local electron gyrofrequency, it follows that the auroral-zone VLF hiss emissions must be generated at relatively low altitudes in the polar magnetosphere, less than 5 R_E for 10 kHz and less than 2 R_E for 100 kHz.

Ellis [1959] first proposed that auroral-zone VLF hiss emissions may be produced by incoherent Cerenkov radiation from the same charged particles that produce auroras. Initial estimates by Ellis based on the limited information about auroral charged-particle energies and fluxes available at that time indicated that the incoherent Cerenkov radiation process was several orders of magnitude too low to explain the observed power fluxes. Later, however, in a more complete analysis based on more recent data, this conclusion was revised by *Jørgensen* [1968], who concluded that VLF hiss could be generated by incoherent Cerenkov radiation from large, but plausible, fluxes of electrons with energies of the order of 1 kev.

Because suitable simultaneous measurements of low-energy charged-particle fluxes and VLF radio noise have not been available, it has not been previously possible to identify the charged particles responsible for the generation of auroral-zone VLF hiss. *Gurnett* [1966], using data from the Injun 3 satellite, made the first quantitative investigation of charged-particle fluxes and their association with auroral-zone VLF hiss. Gurnett found that the VLF hiss emissions were essentially anticorrelated with the intensities of electrons with energies $E \geq 40$ kev, and that the VLF hiss usually occurred on the high-latitude side of the trapping boundary for electrons $E \geq 40$ kev. In a few in-

stances, excellent correlations were found between the occurrence of VLF hiss and very intense fluxes of electrons with energies $E \gtrsim 10$ kev. Generally, however, the charged particles responsible for the auroral-zone VLF hiss emissions could not be detected because of the poor sensitivity and limited energy range of the Injun 3 instrumentation. Recently *Laaspere et al.* [1971] and *Hartz* [1971] have suggested that VLF hiss on the dayside of the magnetosphere is associated wiith an influx of low-energy, 0.1 to 1.0 kev, electrons in a region identified as the 'soft-electron' precipitation zone by *Johnson and Sharp* [1969] and *Eather* [1969]. In this paper we present a study of auroral-zone VLF hiss with charged-particle and VLF instrumentation of suitable sensitivities and dynamic ranges to clearly identify the charged particles responsible for the VLF hiss emissions.

INSTRUMENTATION

The data used in this study were obtained from the NASA/University of Iowa satellite Injun 5. This satellite was launched on August 8, 1968, into an elliptical polar orbit with an inclination of 80.66°, an apogee altitude of 2528 km, and a perigee altitude of 677 km. The satellite carries a tape recorder with a bit rate of 800 bits $(\text{sec})^{-1}$ to provide worldwide spatial surveys and a high bit rate mode of operation at 24,000 bits $(\text{sec})^{-1}$ to provide high temporal resolution measurements of auroral phenomena. The spacecraft is magnetically oriented by a bar magnet within the spacecraft.

The VLF instrumentation on Injun 5 consists of one electric dipole antenna, one magnetic loop antenna, two wide-band (30 Hz to 10 kHz) receivers, and a 6-channel step-frequency receiver covering the frequency range from 7.5 to 105 kHz. The electric and magnetic antennas are mounted in such a way that the Poynting flux direction of the VLF waves, up or down the geomagnetic field, can be determined from the correlation between the electric- and magnetic-field signals. A complete description of the Injun 5 VLF instrumentation is given by *Gurnett et al.* [1969].

Simultaneous measurements of electron and proton intensities within the energy range $5 \leq E \leq 50{,}000$ ev are obtained from two Low-Energy Proton and Electron Differential Energy Analyzers (abbreviated, Lepedea) on Injun 5, one (Lepedea 'A') with a field of view directed antiparallel to the local geomagnetic-field vector and the other (Lepedea 'B') with a field of view directed perpendicular to the local geomagnetic-field vector. Hence Lepedea A measures the precipitated fluxes into the earth's atmosphere over the northern hemisphere and the upgoing fluxes over the southern hemisphere. Energetic electron intensities with energies $E > 45$ kev are surveyed with a companion set of collimated, thin-windowed Geiger-Mueller tubes. Further details of this charged-particle instrumentation are given by *Frank and Ackerson* [1971].

OBSERVATIONS

Survey of VLF Hiss and Associated Plasma Observations

To identify the magnetospheric plasma regime involved in the generation of auroral-zone VLF hiss, a global survey of the VLF/Lepedea data was performed using the tape recorded data. For the data presented in this portion of the study, the Lepedea instrumentation was operated in a special 'survey' mode of operation. This mode of operation provided a high sensitivity over a wide energy range and is particularly suitable for identifying the various plasma regimes in the distant magnetosphere, e.g., polar cap, polar cusp, plasma sheet, and proton ring current. A total of 10 orbits, selected to provide a coarse sampling of all local times, has been analyzed in detail. From these data, 5 polar passes have been selected for presentation in Figures 1 through 5 as representative of the VLF hiss and associated charged-particle fluxes observed.

Figure 1 illustrates an example of an auroral-zone VLF hiss event observed during a polar pass over the northern hemisphere near the noon-midnight meridional plane. The VLF electric-field spectral densities observed on this pass are shown on the top panel of Figure 1 at 3 representative frequencies: 7.35, 22, and 70 kHz. A broad-band VLF noise emission, characteristic of auroral-zone VLF hiss, occurs on this pass from approximately 15h 11m 30s to 15h 13m 30s UT. The VLF hiss spectrum in this case extends from below 7.35 to above 105 kHz, the highest frequency measured, and the integrated broad-band electric-field strength is

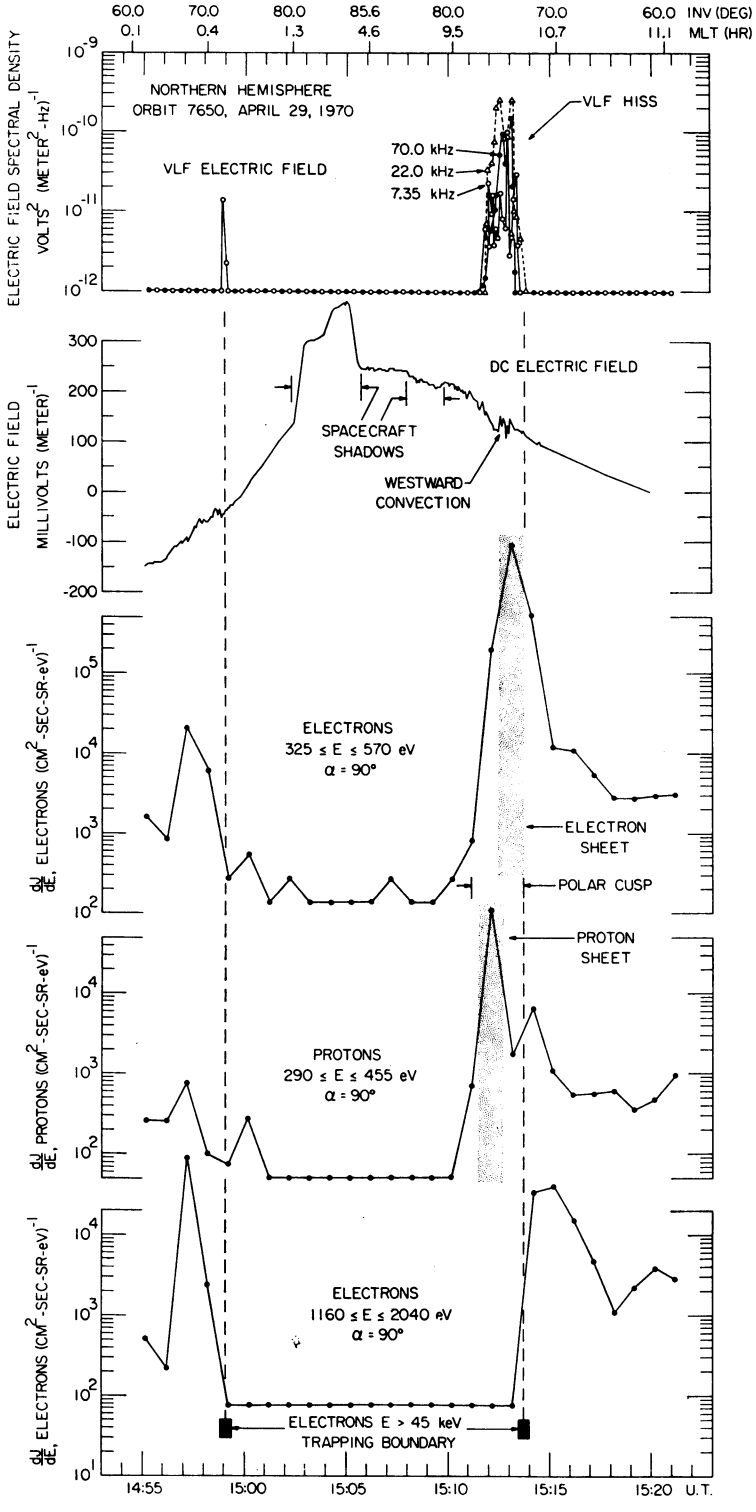
60.0 0.1
70.0 0.4
80.0 1.3
85.6 4.6
80.0 9.5
70.0 10.7
60.0 11.1
INV (DEG)
MLT (HR)
ELECTRIC FIELD SPECTRAL DENSITY VOLTS² (METER²-Hz)⁻¹
NORTHERN HEMISPHERE
ORBIT 7650, APRIL 29, 1970
VLF ELECTRIC FIELD
VLF HISS
70.0 kHz
22.0 kHz
7.35 kHz
ELECTRIC FIELD MILLIVOLTS (METER)⁻¹
DC ELECTRIC FIELD
SPACECRAFT SHADOWS
WESTWARD CONVECTION
ELECTRONS 325 ≤ E ≤ 570 eV α = 90°
ELECTRON SHEET
POLAR CUSP
PROTON SHEET
PROTONS 290 ≤ E ≤ 455 eV α = 90°
ELECTRONS 1160 ≤ E ≤ 2040 eV α = 90°
ELECTRONS E > 45 keV TRAPPING BOUNDARY
14:55
15:00
15:05
15:10
15:15
15:20
U.T.

about 3 mv (meter)$^{-1}$. The magnetic local time (MLT) and invariant latitude (INV) at the time of maximum intensity for this event are about 10.2 hours and 76°, respectively.

During the time when the VLF hiss is observed, the dc electric-field data for this pass show a negative perturbation in the measured dc electric field of about 30 mv (meter)$^{-1}$ from the $\mathbf{V}_s \times \mathbf{B}$ electric field caused by the satellite motion through the ionosphere. This electric-field perturbation corresponds to a westward (antisunward) plasma convection of about 1 km (sec)$^{-1}$ (see *Cauffman and Gurnett* [1971] for a discussion of the Injun 5 dc electric-field experiment and its interpretation).

As shown by the $325 \leq E \leq 570$ ev electron and $290 \leq E \leq 455$ ev proton intensities in Figure 1, the VLF hiss event on this pass occurs in a region of very intense, low-energy (several hundred ev) electron and proton fluxes on the poleward side of the electron $E > 45$ kev trapping boundary. The charged-particle fluxes in this region consist of an equatorward 'electron sheet' and an adjacent poleward 'proton sheet' shown shaded in Figure 1. *Frank* [1971*a*] has recently reported observations of similar proton and electron sheets at high altitudes, $\sim 5\ R_E$, in the dayside polar magnetosphere with the eccentric orbiting satellite Imp 5. The widths of each sheet of $\sim 2°$, the proton and electron intensities, and the relative juxtaposition of these two sheets at low altitudes as shown in Figure 1 are in substantial agreement with the Imp 5 results. These two sheets are identified with the direct entry of magnetosheath plasma into the dayside polar magnetosphere. The corresponding region of direct access of magnetosheath plasma is called the polar cusp [*Frank*, 1971*a*]. Similar low-altitude observations of magnetosheath plasma during local day have been previously reported by *Frank and Ackerson* [1971]. *Heikkila and Winningham* [1971] have also presented detailed observations of this phenomena at low altitudes for a selected pass during very disturbed magnetic conditions ($Kp = 6$; $\Sigma Kp = 41$, $Ap = 54$). The polar-cusp observations of Figure 1, however, are unusual in that (1) the separation of the polar-cusp plasma into distinct proton and electron sheets, commonly observed at high altitudes, is not usually found at low altitudes, and (2) the proton intensities are more intense than usual. On the other hand, this series of observations provides us with a convincing identification of the position of the low-altitude intersection of the polar cusp relative to the various phenomena (e.g., trapping boundary, VLF hiss, plasma convection, etc.) at Injun 5 altitudes.

The very soft energy spectrum of the polar-cusp electrons is illustrated in the bottom panel of Figure 1 by the very low (background level) flux of $1160 \leq E \leq 2040$ ev electrons in the polar-cusp region and over the entire polar-cap region. The abrupt increase in the $1160 \leq E \leq 2040$ ev electron flux at 15h 13m 45s UT marks the transition from the polar-cusp region to the outer radiation zone and is coincident with the trapping boundary for electrons with energies $E > 45$ kev.

From the charged-particle intensities shown in Figure 1, it is evident that the VLF hiss observed on this pass is closely associated with the low-energy polar-cusp plasma. No significant VLF hiss emission is observed in the outer radiation zone, which is characterized by much higher electron energies, or in the polar-cap region, which is essentially void of charged particles with energies $E \gtrsim 50$ ev.

Figures 2 and 3 illustrate two successive polar passes over the southern hemisphere for morning-evening (0800–2000) local times. During the first pass, shown in Figure 2, a very weak VLF hiss event is observed in the local evening (~2100 hours MLT), from about 1536 to 1537 UT, and a much more intense event is observed in the local morning (~0800 MLT), from about 1546 to 1549 UT. On the succeeding pass 2 hours later, shown in Figure 3, the intensity of the VLF hiss has increased con-

Fig. 1. (Opposite) Simultaneous observations of VLF hiss, convection electric fields, and charged-particle fluxes for a noon-midnight meridional pass over the northern auroral-zone and polar-cap region. This pass provides a clear demonstration of the association between the polar-cusp plasma and auroral-zone VLF hiss and illustrates the relative locations of the VLF hiss region, the polar-cusp plasma convection, the polar-cusp electron and proton sheets, and the electron $E > 45$ kev trapping boundary. ($Kp = 2-$.)

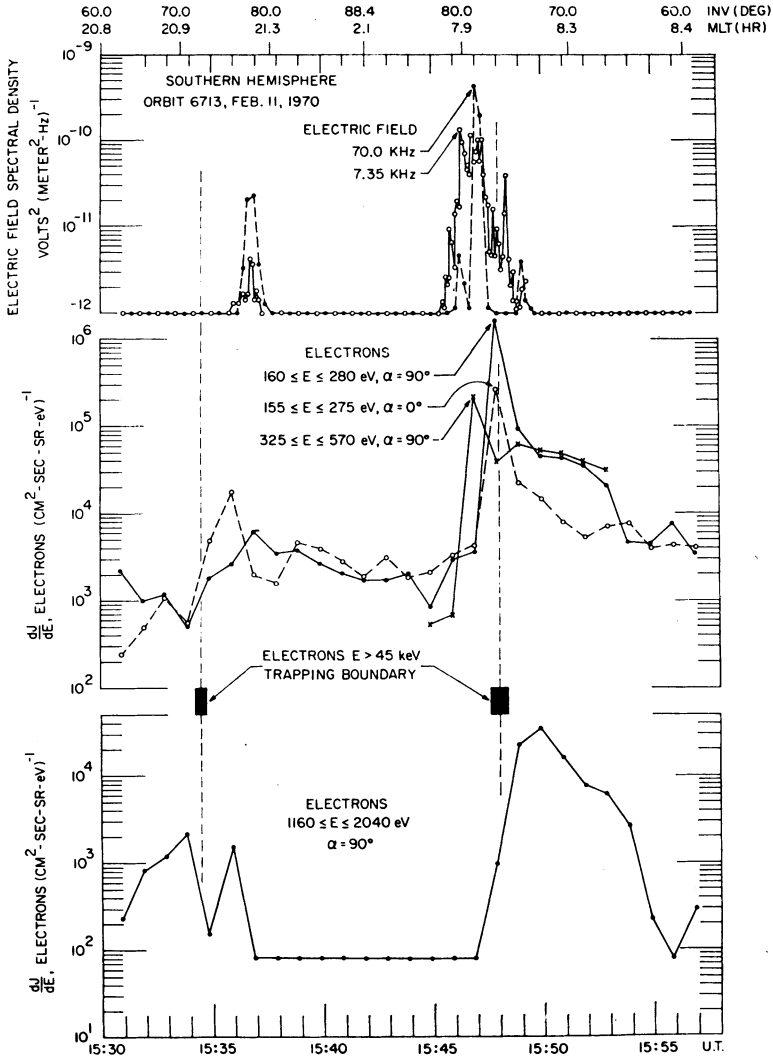

Fig. 2. Simultaneous observations of VLF hiss and intense fluxes of several hundred ev electrons for a morning-evening (0800-2100 MLT) pass over the southern hemisphere. Note the low electron fluxes for the 2100 MLT auroral-zone crossing and the corresponding low VLF hiss intensities. ($Kp = 1-$.)

siderably in the local evening, from 1737 to 1740 UT, and is about the same in the local morning, from 1746 to 1749 UT.

From the corresponding charged-particle intensities shown in Figures 2 and 3, it is evident that the VLF hiss occurs in regions with intense fluxes, $> 10^5$ electrons (cm^2 sec ster ev)$^{-1}$, of low-energy electrons with energies on the order of one to several hundred ev. In the local morning region, these low-energy electrons are again identified by their soft energy spectrum as having originated from the magnetosheath/polar-cusp region. This identification is further supported by the observation of an enhanced flux of $290 \leq E \leq 455$ ev protons from 1747 to 1749 UT in Figure 3 with energy spectra typical of magnetosheath protons. In contrast to the large polar-cusp proton fluxes, $>10^5$ protons (cm^2 sec ster ev)$^{-1}$, observed for the pass in Figure 1, the polar-cusp proton fluxes observed in Figure 3, $\lesssim 10^4$ protons (cm^2 sec ster ev)$^{-1}$, are more typical. It is further noted

that the proton intensities in the VLF hiss region are quite small, at ~1738 UT in Figure 3, for example, thereby identifying the low-energy electrons as the particles responsible for the VLF hiss emission.

The correlation between the occurrence of VLF hiss and the low-energy (few hundred ev) electrons is particularly evident for the local evening auroral-zone crossings in Figures 2 and 3. During the local evening portion of the pass in Figure 2, both the low-energy electron fluxes and the VLF hiss intensities are small. On the following orbit, however, the low-energy electron flux ($160 \leq E \leq 280$ ev, in particular) increases by about 2 orders of magnitude and the broad-band VLF hiss intensity increases accordingly.

In the local evening, the intense fluxes of low-energy electrons observed on the poleward side of the electron $E > 45$ kev trapping boundary, such as from 1737 to 1740 UT in Figure 3, are identified with magnetosheath electron intensities that have been energized by an auroral acceleration process at altitudes $\lesssim 5$ R_E [*Frank and Gurnett,* 1971; *Frank and Ackerson,* 1971]. Further examples of these energetic auroral electron events will be presented and discussed in the following section on high-time resolution observations.

For the southern-hemisphere observations of Figures 2 and 3, Lepedea A, which detects particles with pitch angles of $\alpha = 0°$, is detecting the flux of charged particles coming up the geogmagnetic field from below the satellite. For these passes, the upgoing ($\alpha = 0°$) electron flux is usually less than, or comparable to, the flux perpendicular ($\alpha = 90°$) to the geomagnetic field. Generally these upgoing electron fluxes can be attributed to backscattering of precipitated electrons from the atmosphere below the satellite. However, near the trapping boundary at 17h 49m 30s UT in Figure 3, an intense flux of upgoing $110 \leq E \leq 190$ ev electrons is observed. For this event, the ratio of the upgoing ($\alpha = 0°$) to the perpendicular ($\alpha = 90°$) flux is about 3:1. At higher energies, several hundred ev and above, this anisotropy of electron intensities is not observed. Similar upgoing electron events of this type, sometimes with anisotropy ratios as large as 100:1, are frequently observed with Injun 5.

Figures 4 and 5 illustrate two further examples of auroral-zone VLF hiss and the relevant charged-particle data for successive northern- and southern-hemisphere passes at approximately 0500 and 1700 hours local times. These passes show a marked asymmetry between dawn and dusk local times with VLF hiss occurring at roughly magnetically conjugate locations in the dusk local-time regions. Again the VLF hiss is observed on the poleward side of the electron $E > 45$ kev trapping boundary, and in regions with intense fluxes of electrons with energies on the order of a few hundred ev. For the southern-hemisphere data in Figure 5, intense anisotropic fluxes of upgoing $155 \leq E \leq 275$ ev electrons are evident at 15h 43m 45s and 15h 45m 50s UT. The measurements of electron intensities at $\alpha = 0°$ ($155 \leq E \leq 275$ ev) and 90° ($160 \leq E \leq 280$ ev) are simultaneous. The ratio of the upgoing ($\alpha = 0°$) to the perpendicular ($\alpha = 90°$) flux for the event at 14h 45m 50s UT is approximately 100:1.

High–Temporal Resolution Observations

In this section, observations from several high bit rate passes over the auroral zone are presented to illustrate the detailed spatial and temporal structure of VLF hiss and related phenomena. For this portion of the study, a total of about 20 high bit rate passes has been investigated at various local times to determine the details of the charged-particle/VLF relationships. The passes selected for presentation have been chosen to illustrate a variety of effects observed.

Observations near local noon. Plate 1 shows a color-coded energy-time spectogram of the precipitated electron flux observed for a high bit rate pass through the polar-cusp region at about 1020 MLT (see *Frank and Ackerson* [1971] for details concerning the energy-time spectrogram display). On this pass the trapping boundary for electrons $E > 45$ kev occurred at about 23h 30m 50s UT. At latitudes equatorward of the trapping boundary, the electron energy spectrum is relatively hard with energies (1–10 kev) typical of the outer radiation zone at these local times [*Frank and Ackerson,* 1971]. Near the trapping boundary at about 23h 31m 00s UT, a brief (4 sec) intense flux, $\sim 10^9$ electrons $(\text{cm}^2 \text{ sec ster})^{-1}$, of low-energy (~100 ev) electrons is observed. These

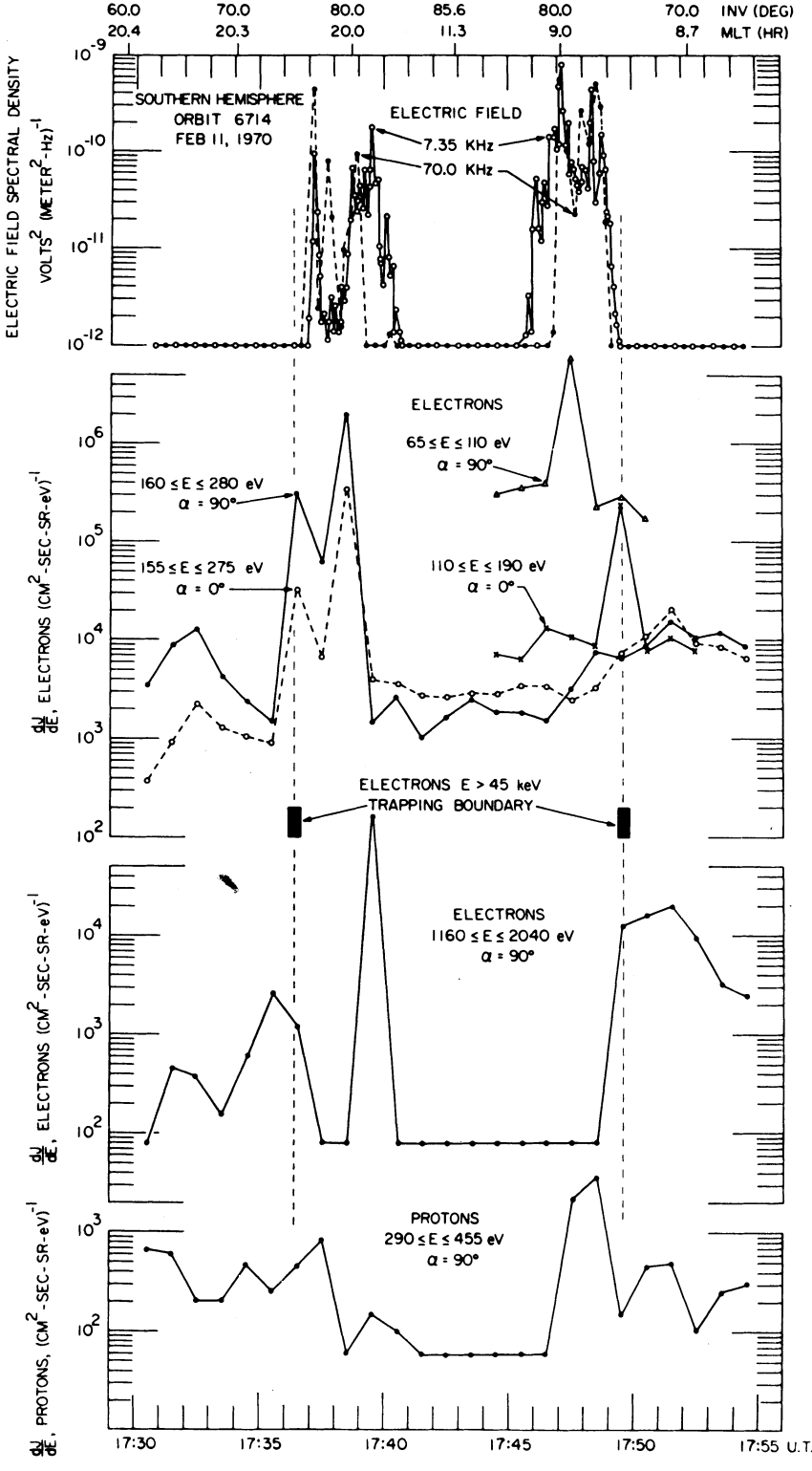
60.0 70.0 80.0 85.6 80.0 70.0 INV (DEG)
20.4 20.3 20.0 11.3 9.0 8.7 MLT (HR)
ELECTRIC FIELD SPECTRAL DENSITY VOLTS² (METER²-Hz)⁻¹
SOUTHERN HEMISPHERE
ORBIT 6714
FEB 11, 1970
ELECTRIC FIELD
7.35 KHz
70.0 KHz
ELECTRONS
65 ≤ E ≤ 110 eV
α = 90°
160 ≤ E ≤ 280 eV
α = 90°
155 ≤ E ≤ 275 eV
α = 0°
110 ≤ E ≤ 190 eV
α = 0°
dJ/dE, ELECTRONS (CM²-SEC-SR-eV)⁻¹
ELECTRONS E > 45 keV
TRAPPING BOUNDARY
ELECTRONS
1160 ≤ E ≤ 2040 eV
α = 90°
dJ/dE, ELECTRONS (CM²-SEC-SR-eV)⁻¹
PROTONS
290 ≤ E ≤ 455 eV
α = 90°
dJ/dE, PROTONS, (CM²-SEC-SR-eV)⁻¹
17:30 17:35 17:40 17:45 17:50 17:55 U.T.

low-energy electrons continue to be observed with reduced intensities, $\sim 3 \times 10^7$ electrons (cm^2 sec ster)$^{-1}$, until, at approximately 23h 32m 10s UT, the flux abruptly decreases to a low level typical of the polar-cap region. On the basis of their energy spectra, intensities, angular distributions, and location relative to the trapping boundary and polar-cap region, these low-energy electrons are identified as having originated from the dayside magnetosheath and the corresponding region, from 23h 31m 00s to 23h 32m 10s UT, is identified as the polar cusp.

Further evidence of the polar-cusp location in this case is provided by the dc electric-field data shown in Figure 6. The sinusoidal variation of the measured electric field with a period of about 8 min is caused by the satellite rotation in the $\mathbf{V}_s \times \mathbf{B}$ field. A 50- to 100-mv/m perturbation of the measured electric field from the $\mathbf{V}_s \times \mathbf{B}$ field is observed from 23h 31m 00s to 23h 32m 00s UT, in almost exact correspondance with the polar-cusp region identified with the charged-particle data. This electric field corresponds to an eastward plasma convection of about 1.5 to 3.0 km/sec. This convection direction is in contrast to the westward convection direction observed for the pass in Figure 4. Eastward convection indicates that in this case the 'stagnation point' for the east-west plasma flow in the polar-cusp region is on the dawnside of the magnetosphere at a magnetic local time less than 1020 MLT. For further details on high-latitude plasma convection observations with Injun 5, the reader is referred to *Cauffman and Gurnett* [1971].

The frequency-time spectra of the VLF electric and magnetic fields observed during this pass are shown in Figure 7. In the outer radiation zone region, at latitudes equatorward of the trapping boundary for electrons $E > 45$ kev, the primary VLF noise observed is chorus and ELF hiss. At the trapping boundary the chorus and ELF hiss emissions disappear and the spectrum changes abruptly to VLF hiss with impulsive temporal structure characteristic of VLF hiss near local noon [*Gurnett*, 1966]. The region of maximum intensity for the auroral hiss emission corresponds well with the polar-cusp region identified from the charged-particle and convection electric-field data. The maximum broad-band (300 Hz to 10 kHz) VLF electric- and magnetic-field intensities in this case are approximately 0.53 mv (meter)$^{-1}$ and 1.8 mγ, respectively. The increased intensity of the electric-field spectra as compared with the magnetic-field spectra, evident in Figure 7, is mainly attributed to the greater sensitivity of the Injun 5 electric antenna as compared with that of the magnetic antenna.

Observations near local evening. The charged-particle and VLF data observed for a high bit rate pass over the northern auroral zone in the local evening at approximately 2200 MLT are shown in Plates 2 and 4. During this pass, a moderately intense auroral electron precipitation event occurred from about 04h 05m 20s to 04h 06m 20s UT as shown by the Lepedea A energy-time spectrogram in Plate 2. This event was characterized by relatively low electron energies, primarily less than 1 kev, and maximum electron fluxes of about 2×10^9 electrons (cm^2 sec ster)$^{-1}$. On this pass the electron $E > 45$ kev trapping boundary occurred at about 04h 06m 20s UT, coincident with the equatorward boundary of the electron precipitation region.

Using the correlation techniques described by *Gurnett et al.* [1971] the VLF electric- and magnetic-field signals for this pass have been processed to produce color frequency-spectrograms of waves propagating up (red) and down (green) the geomagnetic field as shown in Plate 4. From these spectrograms it is evident that two distinct types of VLF noise occurred in association with the electron precipitation event shown in Plate 2. The green (downgoing) VLF hiss emission has a frequency spectrum that is more or less typical of VLF hiss observed in the local evening [*Gurnett*, 1966]. The temporal/spatial location of this downgoing VLF hiss event corresponds almost exactly (± 10 sec) with the region of maximum electron precipitation shown in Plate 2.

Fig. 3. (Opposite) Continuation of Figure 2 for the following southern-hemisphere pass approximately 2 hours later. Note the greatly increased flux of low-energy, several hundred ev, electrons for the 2100 MLT auroral-zone crossing as compared with Figure 2 and the corresponding increase in the VLF hiss intensity. An intense flux of upgoing ($\alpha = 0°$), $110 \leq E \leq 190$ ev, electrons is observed near the trapping boundary at 17h 49m 30s UT.

The power flux of the VLF hiss in this event can be estimated by using the Poynting flux measurement theory of *Mosier and Gurnett* [1971]. For the Injun 5 antenna configuration it can be shown that the correlation, $\langle E_x H_y \rangle$, between the electric, E_x, and magnetic, H_y, field signals is proportional to the average Poynting flux component, $\langle S_z \rangle$, parallel to the geomagnetic field, $\langle E_x H_y \rangle = G(\mathbf{K}) \langle S_z \rangle$. The proportionality factor $G(\mathbf{K})$ is a function of the wave normal direction and is not known precisely because the wave normal direction is generally unknown. It can be shown, however, that $G(\mathbf{K})$ is always positive and less than 1 at VLF frequencies and

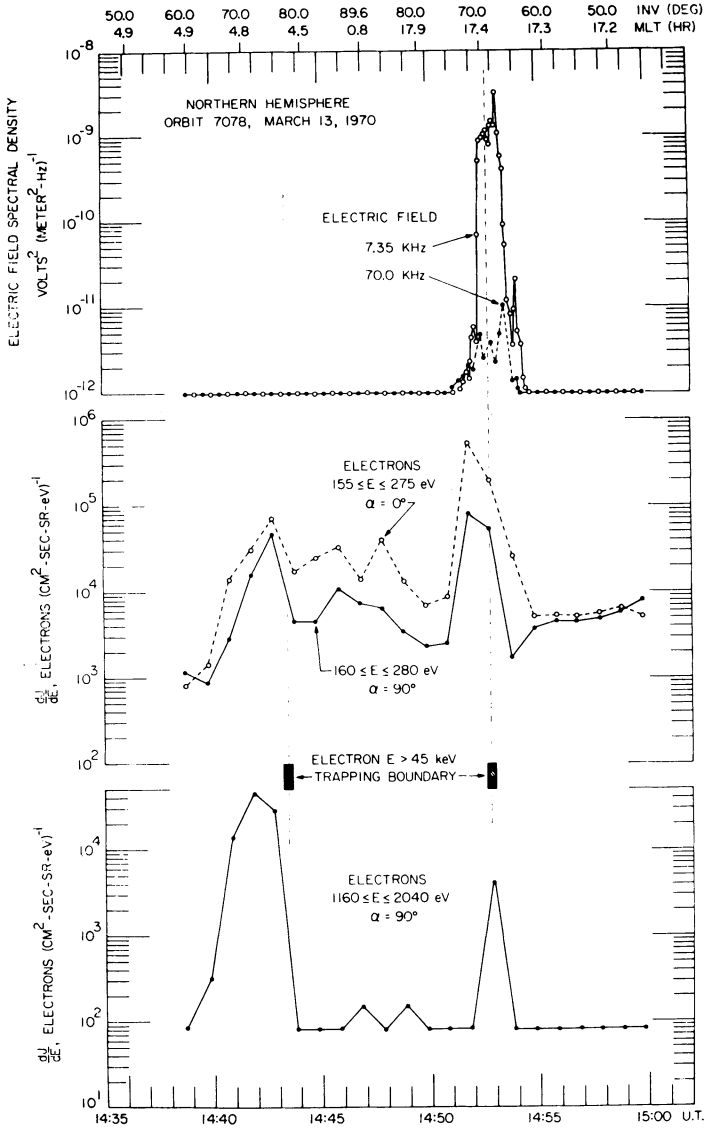

Fig. 4. Observations of VLF hiss and associated low-energy electron fluxes for a dawn-dusk (0500–1700 MLT) pass over the northern hemisphere. Note the asymmetry between dawn and dusk local times. Inverted V electron precipitation bands centered at ~1443 and 1453 UT have been previously identified by *Frank and Gurnett* [1971]. The precipitation band at local morning is unusual in the fact that the fluxes of low-energy electrons $E > 50$ ev were $\sim 10^8$ (cm² sec ster)$^{-1}$, approximately a factor of 10 less than is typically observed in these events. ($Kp = 3-$.)

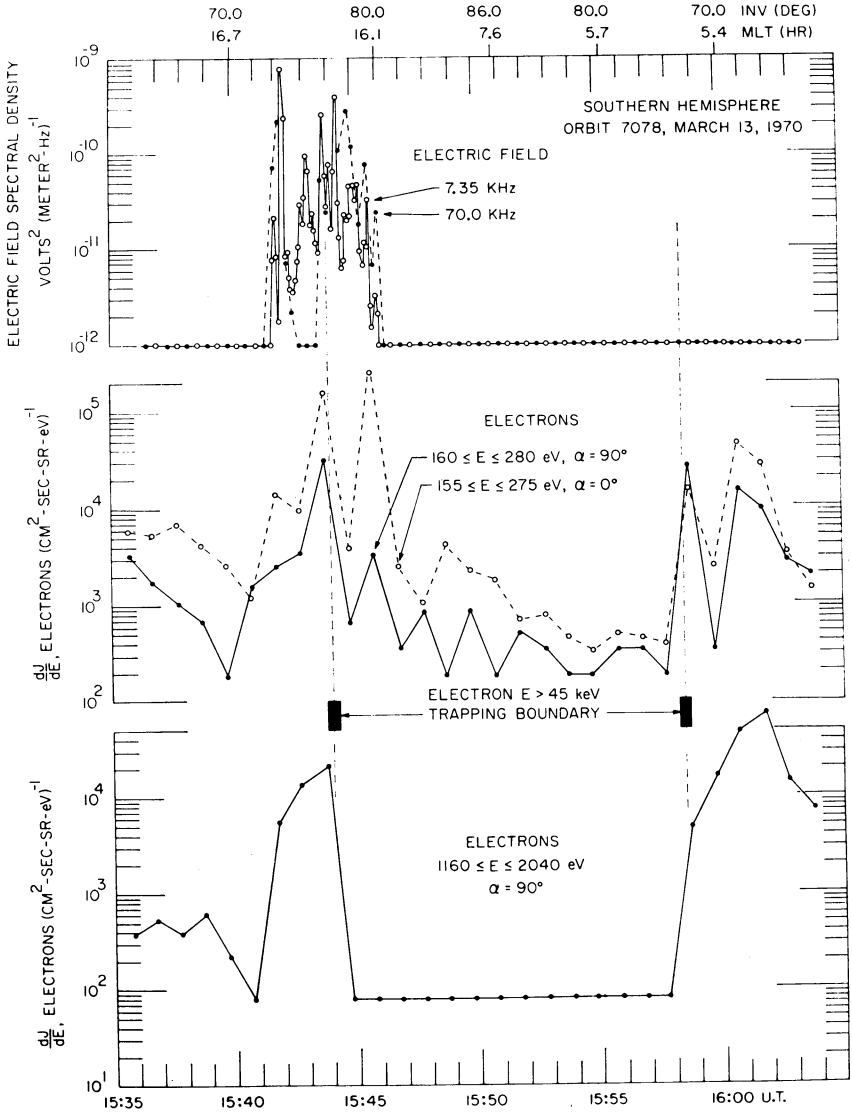

Fig. 5. Continuation of Figure 4 for the following southern-hemisphere pass approximately 1 hour later ($Kp = 2+$.)

that the average value of $G(\mathbf{K})$, averaged over all wave directions, is $\frac{1}{2}$. We can therefore place a lower limit on the Poynting flux of $\langle S_z \rangle \geq \langle E_x H_y \rangle$ and can make a best estimate for the Poynting flux of $\langle S_z \rangle \simeq 2 \langle E_x H_y \rangle$. The correlation $\langle E_x H_y \rangle = |E_x|\,|H_y| \langle \cos \phi \rangle$ is determined most accurately from the Injun 5 telemetry by using the electric- and magnetic-field strength measurements made on board, $|E_x|$ and $|H_y|$, and by measuring the average value of the cosine of the phase angle between the electric- and magnetic-field signals, $\langle \cos \phi \rangle$, from the wide-band telemetry. For the VLF hiss event shown in Plate 4 the broad-band, 300 Hz to 10 kHz, electric- and magnetic-field strengths at the time of maximum intensity (04h 05m 48s UT) are 1.67 mv $(\mathrm{m})^{-1}$ and 11.4 mγ, respectively, and the cosine correlation $\langle \cos \phi \rangle$ is approximately 0.7. Using an effective noise bandwidth for the emission of 5 kHz, the corresponding lower limit on the VLF power flux for this event is 2.0×10^{-12} watts $(\mathrm{m}^2\ \mathrm{Hz})^{-1}$.

The actual power flux is larger, probably on the order of 4.0×10^{-12} watts $(m^2\ Hz)^{-1}$.

Following the downgoing VLF hiss event in Plate 4, an upgoing (red) VLF emission called a saucer is observed. Saucers are characterized by a parabola-shaped appearance on a frequency-time spectrogram, typically with a duration of about 10 sec or less, and are invariably observed to be propagating up the geomagnetic field from below the satellite [*Mosier and Gurnett,* 1969]. In contrast to the downgoing VLF hiss, the saucer is not located in the region of maximum electron precipitation but rather is located at the equatorward boundary of the electron precipitation event and near the electron $E > 45$ kev trapping boundary. This relationship is typical of most saucers observed with Injun 5, in that saucers do not normally occur in the region of most intense electron precipitation, but rather occur at the boundary of a precipitation band. Saucers have been observed in situations where no downgoing electron or proton fluxes, $E >$ 50 ev, above the background level of the Lepedea instrumentation and with an appropriate duration, 10 sec, could be associated with the saucer emissions. Unfortunately, because of limitations on receiving the high bit rate and broad-band VLF telemetry, no suitable data are available from the southern hemisphere, where Lepedea A views particles coming up the geomagnetic field from the ionosphere, to investigate the possibility that saucers may be caused by upgoing electrons. The possibility that saucers may be associated with upgoing low-energy electrons is considered further in the interpretation and discussion section of this paper.

The charged-particle and VLF data observed during another pass at about 1900 MLT in the local evening are shown in Plates 3 and 5. The low-energy electron precipitation region observed with Lepedea A during this pass is very broad, extending from approximately 22h 54m 15s to 22h 56m 50s UT. The electron energy-time spectrogram for this pass shows a series of inverted 'V' structures of the type identified by *Frank and Ackerson* [1971]. The average electron energy in these inverted V events extends to several kev, and the maximum electron fluxes are about 1.6×10^9 electrons $(cm^2\ sec\ ster)^{-1}$. The electron $E > 45$ kev trapping boundary occurs near the end of the pass at 22h 57m 50s UT equatorward of the intense low-energy electron precipitation. A detailed discussion of this series of observations and representative spectra are given in the survey by *Frank and Ackerson* [1971].

The VLF frequency-time spectrograms for this pass again show distinctly different phenomena propagating up and down the geomagnetic field. Downgoing (green) V-shaped VLF hiss events are observed at about 22h 55m 10s and 22h 56m 00s UT. V-shaped VLF hiss events of this type have been previously discussed by *Gurnett* [1966] and are the most common spectral form of VLF hiss observed during local evening. V-shaped VLF hiss events can be distinguished from saucers on the basis of their duration, which, for the Injun 5 orbit, is typically about 1 min (or 500 km latitudinal width). The broad-band electric- and magnetic-field strengths observed for the first V-shaped hiss event at 22h 55m 10s UT are about 4.2 mv $(m)^{-1}$ and 10.0 mγ, respectively, and the cosine correlation, $\langle \cos \phi \rangle$, is about 0.5. The corresponding VLF power flux for this event is at least 5.5×10^{-12} watt $(m^2\ Hz)^{-1}$, and probably about 1.1×10^{-11} watt $(m^2\ Hz)^{-1}$. From the charged-particle and VLF spectrograms in Plates 3 and 5, it is evident that the downgoing V-shaped VLF hiss events occur in the same region as the inverted V electron precipitation events. The similarity in the duration and relative locations of the V-shaped hiss events and the inverted V electron precipitation events shows that these phenomena are closely related. In general, for this and other similar cases, the detailed temporal (or spatial) features of these two phenomena are not always coincident on time (or distance) scales of less than about 10 sec (100 km). However, since the VLF hiss is probably generated well above the Injun 5 altitude and the VLF ray paths do not necessarily follow the charged-particle trajectories, this lack of a detailed correspondence in all cases is not surprising.

Following the V-shaped VLF hiss events in Plate 5, an upgoing (red) saucer emission is observed at approximately 22h 58m 00s UT. Again the saucer emission is observed near the boundary of the primary electron precipitation region, and no clearly identifiable feature in the precipitated electron spectrum with a time

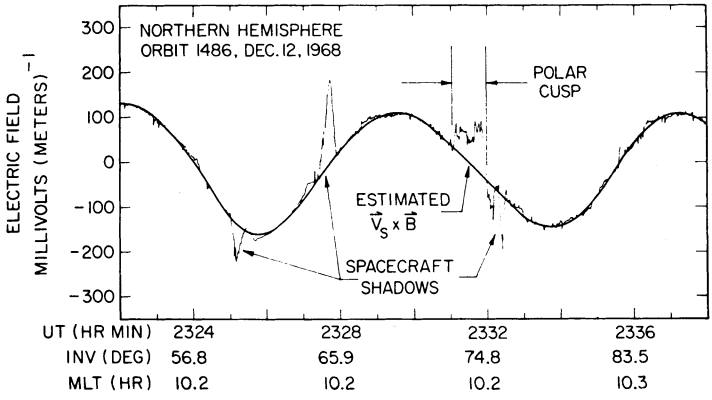

Fig. 6. Convection electric-field observations for the polar-cusp crossing in Plate 1. The $\mathbf{V_s \times B}$ field is caused by the spacecraft motion through the ionosphere. The electric-field perturbation from the $\mathbf{V_s \times B}$ field, from 23h 31m 00s to 23h 32m 00s UT, corresponds to an eastward plasma convection in the polar-cusp region.

scale comparable to or less than the saucer duration can be associated with the saucer.

SUMMARY OF OBSERVATIONS

A variety of examples of auroral-zone VLF hiss and related plasma phenomena in the polar magnetosphere has been presented. On the basis of these and other examples investigated but not presented here, we summarize below the principal observational results of this study.

1. Auroral-zone VLF hiss is observed near and on the poleward side of the 'trapping boundary' for energetic electrons $E > 45$ kev in a zone typically about 7° wide in latitude, centered on 77° INV at local noon, and decreasing to 72.0° INV at local midnight. The electron $E > 45$ kev trapping boundary is observationally identified with the high-latitude termination of measurable electron $E > 45$ kev intensities.

2. In this region near and poleward of the electron $E > 45$ kev trapping boundary, VLF hiss is associated with intense fluxes of precipitating low-energy electrons with energies on the order of 100 ev to several kev. On the dayside of the magnetosphere, the region where these low-energy electron fluxes and the associated VLF hiss are observed is identified as the dayside polar cusp. On the nightside of the magnetosphere, the corresponding region of occurrence of VLF hiss is identified with the downstream magnetosheath and the distant plasma sheet, which are the topological extensions of the polar cusp into the magnetotail.

3. A pronounced day-night asymmetry exists in the occurrence and spectral character of both the VLF hiss and the associated low-energy electron flux (see Figures 1 through 5, Figure 7, and Plate 4). During the local day, detectable levels of VLF hiss and low-energy electron fluxes are essentially omnipresent in the polar-cusp region. The electron energy spectrum in the dayside polar cusp is normally very soft (~100 ev) and shows relatively little evidence of acceleration or heating of the magnetosheath electrons. The VLF hiss frequency-time spectrum in the dayside polar cusp is characterized by rapid temporal variations of all frequencies on a time scale of a few seconds (see Figure 7) and is called impulsive VLF hiss by *Gurnett* [1966]. During the local evening, the VLF hiss intensities and the low-energy electron intensities are highly variable (see Figures 2 and 3). The electron energy spectrum in the local evening is characterized by inverted V precipitation events and shows considerable evidence of acceleration and heating. The VLF hiss spectrum in the local evening often shows a V-shaped frequency-time structure (see Plate 5). In many instances where multiple inverted V events occur, there appears to be a close correspondence between individual inverted V events and the V-shaped VLF hiss events.

4. There is evidence of a significant dawn-dusk asymmetry in the occurrence of VLF hiss and the spectral characteristics of the precipitated electrons. In particular, in the early morning region from 0000 to 6000 MLT, both VLF hiss and the inverted V electron precipitation events are relatively uncommon.

5. VLF hiss is generally observed to be propagating down the geomagnetic field from a generation region above the spacecraft. The power flux of VLF hiss is sometimes as large as 10^{-12} to 10^{-11} watt $(m^2\ Hz)^{-1}$. The corresponding energetic charged-particle fluxes observed for the VLF hiss events of this intensity have energies on the order of 100 ev to several kev and fluxes of about 10^9 electrons $(cm^2\ sec\ ster)^{-1}$ (see, for example, the discussion of Plates 2 and 3).

6. Some evidence indicates that there is a 'threshold' low-energy electron flux below which VLF hiss is not observed. A cursory examination of Figures 1 through 5, as well as other examples investigated but not shown, indicates that when the ~100-ev electron flux is less than about 10^4 to 10^5 electrons $(cm^2\ sec\ ster\ ev)^{-1}$, there is little or no VLF hiss present. When the low-energy electron flux is above this 'threshold,' VLF hiss is essentially always observed; however, the VLF hiss intensity is not necessarily proportional to the low-energy charged-particle flux (see Figures 1 and 4).

7. Intense highly anisotropic fluxes of upgoing low-energy (~ 100 ev) electrons, $j(\alpha = 0°)/j(\alpha = 90°) \gg 1$, are frequently observed in the VLF hiss region. These upgoing low-energy electrons occur in a very narrow zone, less than ~2° in latitudinal width, usually comprising only one measurement (1-min time resolution) in the low bit rate tape-recorded data (see Figure 5). The absence of high bit rate telemetry coverage in the southern hemisphere, where Lepedea A views upcoming particles, prevents us from investigating these events with higher time resolution in this study. However, an analysis of high bit rate data during the period immediately following launch for which the spacecraft was spinning before magnetic stabilization occurred is currently being made and should yield more information concerning the upgoing electron fluxes.

8. Near the boundary of the low-energy electron precipitation regions associated with the downgoing VLF hiss, a type of VLF radio noise called a saucer is often observed propagating up the geomagnetic field from a generation region below the satellite. These saucer emissions are always of short duration, typically 10 sec or less, and are suggestive of a very narrow (~ 100 km) latitudinal source width. In no case has it been possible to associate a charged particle precipitation event ($E > 50$ ev) of corresponding duration as, and simultaneous with, a saucer. Although it is considered likely that the saucer emissions are associated with the upgoing electrons discussed earlier, this relationship cannot be confirmed because of the limited broad-band VLF data available from the southern hemisphere, where these upgoing electron fluxes can be detected.

DISCUSSION AND INTERPRETATION

The results of this study provide a direct verification of the association between auroral-zone VLF hiss and intense fluxes, 10^4 to 10^7 electrons $(cm^2\ sec\ ster\ ev)^{-1}$, of low-energy electrons with energies on the order of 100 ev to several kev. On the dayside of the magnetosphere, these low-energy electrons are identified with the dayside polar-cusp region observed by *Frank* [1971*a*] at higher altitudes with the Imp 5 satellite. At other local times, through the dawn and dusk regions and into the nightside of the magnetosphere, the VLF hiss and associated low-energy electron precipitation regions are believed to correspond to the longitudinal extension of the dayside polar-cusp plasma into the distant plasma sheet and downstream magnetosheath on the nightside of the magnetosphere, following the observational model of *Frank* [1971*b*]. As discussed by *Frank* [1971*a*, *b*], the magnetic-field lines throughout this region of low-energy electron precipitation are 'open,' thereby providing for the direct entry of magnetosheath plasma. Low-altitude observations by *Frank and Gurnett* [1971] show that this region is also characterized by antisolar plasma flow reflecting the bulk motion of magnetosheath plasma past the earth. On the nightside of the magnetosphere significant acceleration of the magnetosheath electrons is observed, as characterized by the inverted *V* electron precipitation events. As discussed by *Frank and Gurnett* [1971], the character of these electron precipitation events suggests that the electron acceleration is caused by quasi-

static electric fields parallel to the geomagnetic field at altitudes $\lesssim 5\ R_E$.

The observation of a significant energy spread for the electron spectra within these inverted V precipitation bands, sometimes comparable to the average energy of the electron spectra, indicates that considerable heating or scattering of the precipitated electron beam must occur if the primary acceleration process is due to quasi-static electric fields. The association of intense VLF hiss with inverted V electron precipitation events suggests that VLF hiss may be closely related to this heating process. A variety of instability mechanisms is known which could cause the observed heating and VLF hiss generation [i.e., *Kindel and Kennel*, 1971]. The absence of any detectable precipitating charged-particle flux, $E < 50$ ev, with a latitudinal width (<10 km) suitable for explaining the saucer emissions, the correspondingly narrow latitudinal width and region of occurrence of the saucer emissions, and the intense fluxes of upgoing low-energy electrons commonly observed near the inverted V electron precipitation regions provide us with some evidence that saucers are generated by these upgoing electrons.

The generation of VLF hiss by incoherent Cerenkov radiation, as proposed by *Jørgensen* [1968], *Hartz* [1971], and others, is considered unlikely as a general process for explaining VLF hiss because of the large power fluxes sometimes observed. This difficulty with the incoherent Cerenkov radiation mechanism is illustrated, for example, by the event in Plates 3 and 5, which has an electron energy spectrum at the peak of the inverted V very similar to that used by *Jørgensen* [1968] for a calculation of the VLF power flux due to Cerenkov radiation. The power flux of the VLF hiss in this event is observed to be greater than 5×10^{-12} watt $(m^2\ Hz)^{-1}$, whereas Jørgensen's model calculations indicate a maximum power flux of about 10^{-14} watt $(m^2\ Hz)^{-1}$, thus leaving a discrepancy of about a factor of 500 between the computed and observed power fluxes. Similar conclusions are obtained for the event in Plates 2 and 4 after corrections are included for the lower average electron energies and increased Cerenkov radiation expected in this case. These intense events, although probably not representative of the 'average' intensity of a VLF hiss event, serve to illustrate the difficulties of explaining all the observed VLF hiss emissions by an incoherent radiation process. The aforementioned evidence of a threshold electron flux necessary for the generation of VLF hiss appears to be also indicative of a coherent plasma instability, and not an incoherent process, operative in some, if not all, of these events.

The configuration envisioned for the generation of VLF hiss and saucer emissions is illustrated in Figure 8. This model is intended to explain the main observational features of local evening events similar to those shown in Plates 4 and 5. In this model, downgoing VLF 'auroral hiss' is generated at an altitude above the satellite by downgoing magnetosheath electrons that have been accelerated to form an inverted V electron precipitation event. At a lower latitude, near or at the boundary between 'open' and 'closed' field lines, an upgoing saucer emission is generated below the satellite by the upgoing ionospheric electron flux that forms the return current. That such a field-aligned current configuration does occur can only be inferred indirectly from the Injun 5 measurements; however, *Cloutier et al.* [1970] have observed an essentially identical current configuration with rocket-borne magnetometers over an auroral arc in the local evening. Although the detailed generation mechanism for the saucer is not known, the frequency-time shape of the saucer can be explained in some detail by the frequency dependence of the limiting ray angle for whistler mode propagation from the generation region to the satellite [*Mosier and Gurnett*, 1969]. From the frequency-time envelope of a saucer, Mosier and Gurnett have estimated the source location for a representative saucer to be about 1100 km below the satellite and at an altitude of about 1400 km. The general similarity in the spectral form of saucers and V-shaped VLF hiss events suggests that the V-shaped form of the VLF hiss observed in the local evening is also caused by the same limiting ray angle effect for downgoing Whistler mode waves. If this is the case, then a coarse estimate for the height of the VLF hiss generation region above the satellite is given by 1100 km times (latitudinal width of a V-shaped VLF hiss event/latitudinal width of a saucer). This rough estimate typically places the VLF hiss generation region at an altitude of about 5000 to 10,000 km. If the VLF hiss is associated with the heating of the precipitated electrons, it is

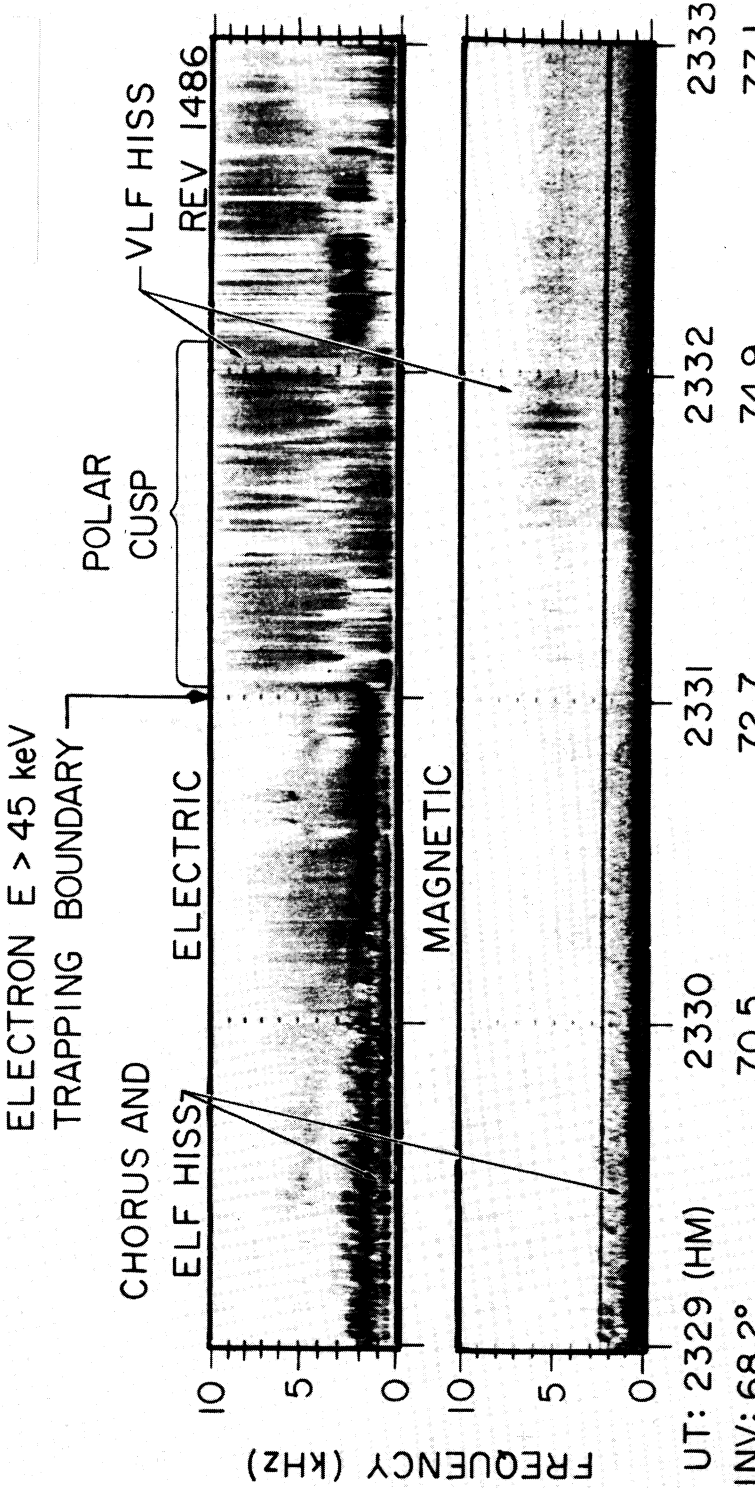

Fig. 7. VLF electric and magnetic frequency-time spectrograms for the polar-cusp crossing in Plate 1, showing the occurrence of chorus and ELF hiss equatorward of the $E > 45$ kev trapping boundary and VLF hiss in the polar-cusp region.

Plate 1. Lepedea A energy-time spectogram for a northern-hemisphere pass through the polar-cusp region near local noon (1000 MLT). The electron $E > 45$ kev trapping boundary is located at about 23h 30m 50s UT, and the region from 23h 31m 00s to 23h 32m 10s UT is identified as the polar cusp. ($Kp = 3$.)

Plate 2. Lepedea A energy-time spectogram of an intense 2×10^9 electrons $(cm^2\ sec\ ster)^{-1}$, low-energy $E \gtrsim 1$ kev, electron precipitation event in the local evening (2200 MLT). The electron $E > 45$ kev trapping boundary is at 04h 06m 20s UT. ($Kp = 0+$.)

Plate 3. Lepedea A energy-time spectogram showing a series of inverted V electron precipitation events from 22h 54m 15s to 22h 56m 50s UT. The electron $E > 45$ kev trapping boundary is at 22h 57m 50s UT. ($Kp = 2-$.)

Plate 4. Frequency-time spectograms showing downgoing (green) VLF hiss and an upgoing (red) saucer emission associated with the low-energy electron precipitation event in Plate 2. Note that the VLF hiss occurs in the region of most intense electron flux, whereas the saucer occurs at the equatorward boundary of the precipitation region and near the electron $E > 45$ kev trapping boundary.

Plate 5. Frequency-time spectograms showing two downgoing (green) V-shaped VLF hiss events and an upgoing (red) saucer emission associated with the inverted V precipitation events shown in Plate 2.

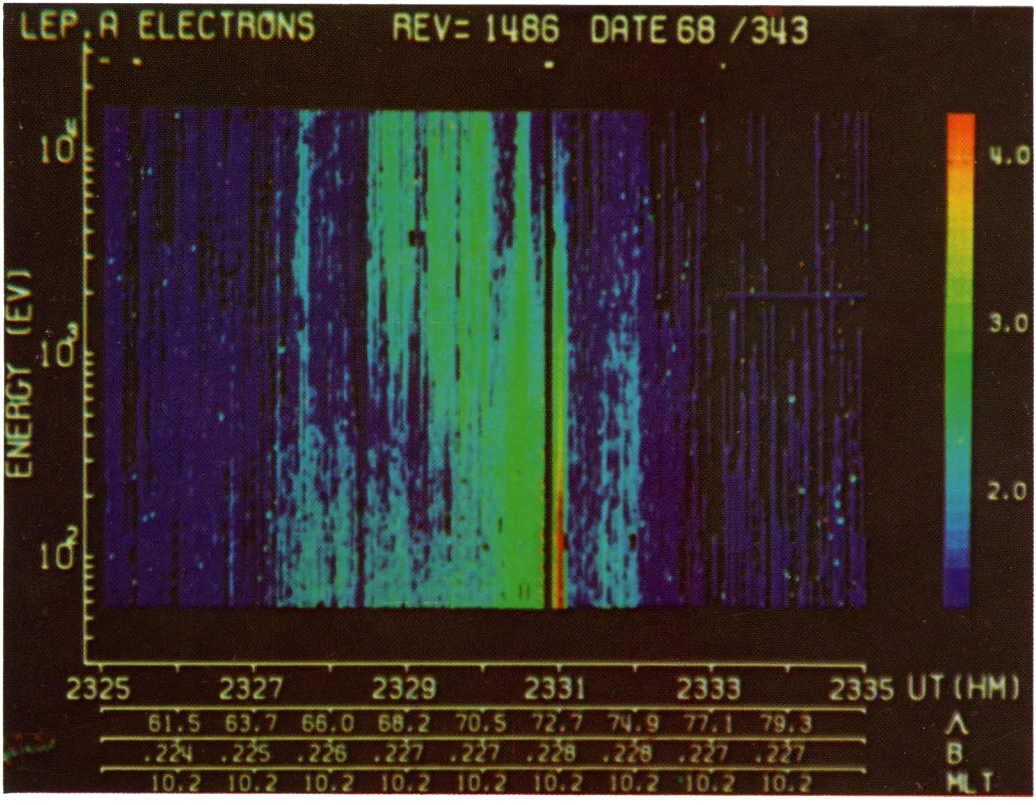

Plate 1.

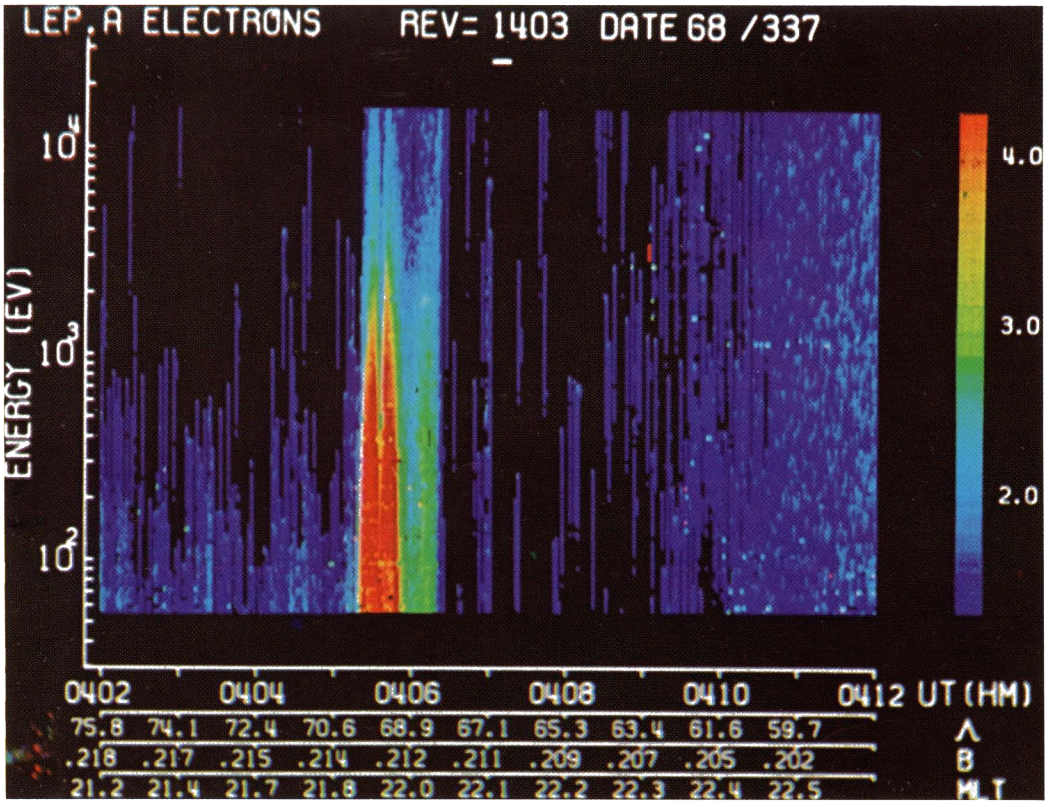

Plate 2.

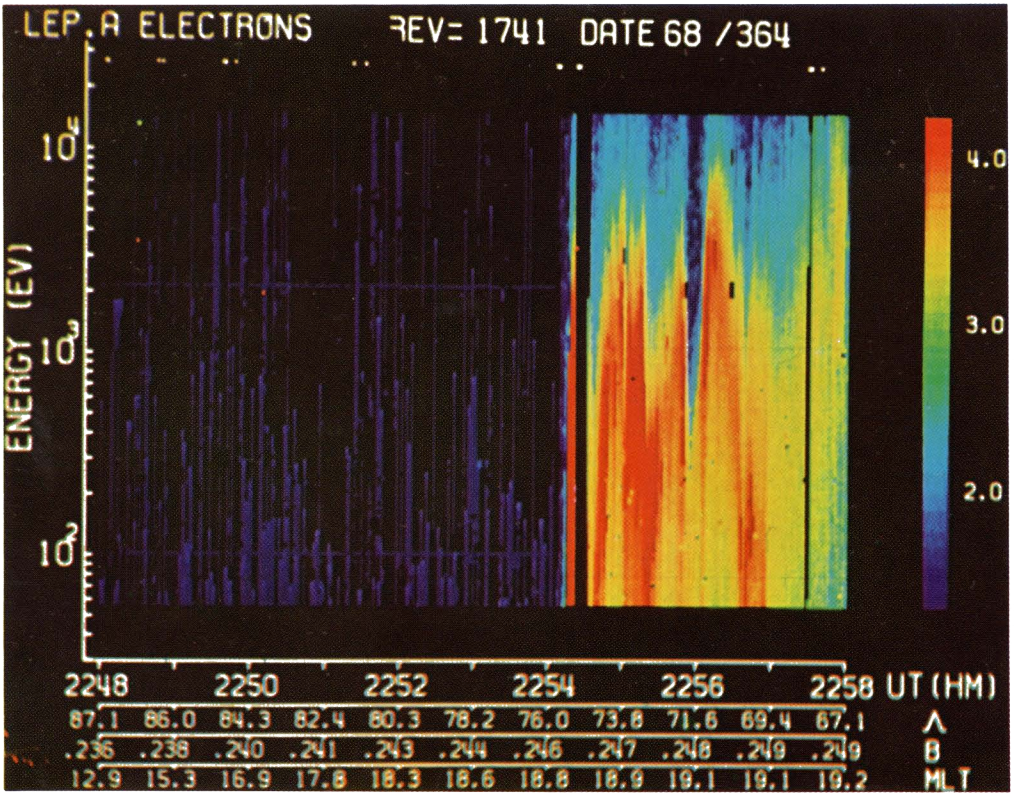

Plate 3.

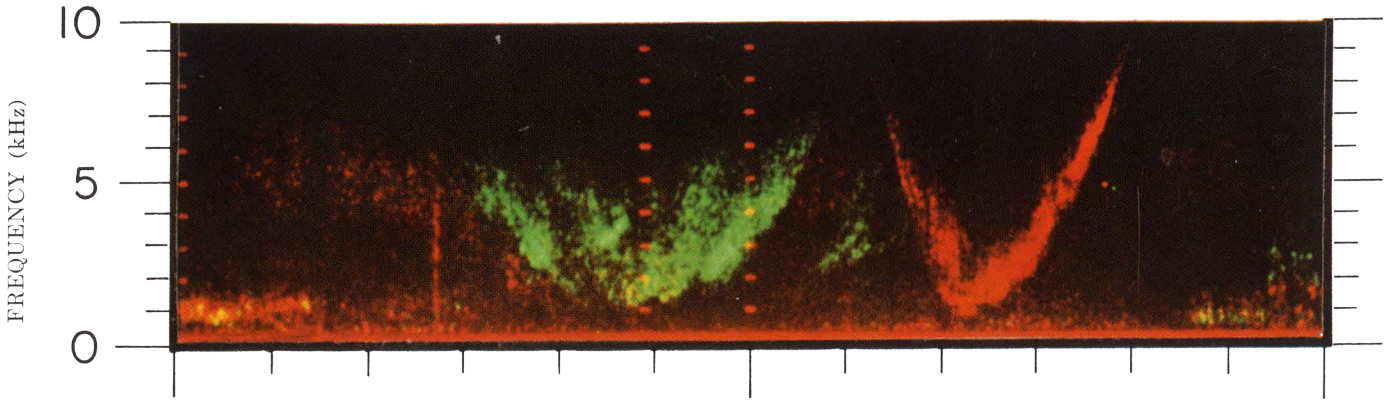

Plate 4.

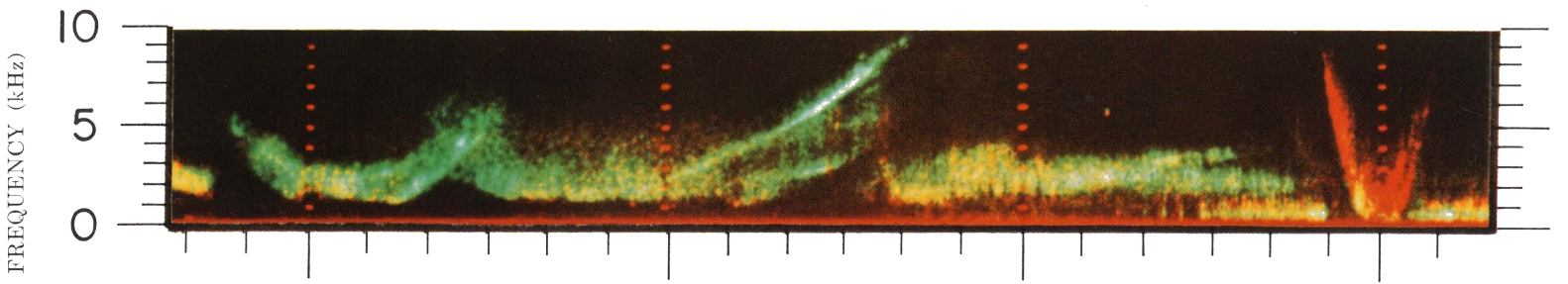

Plate 5.

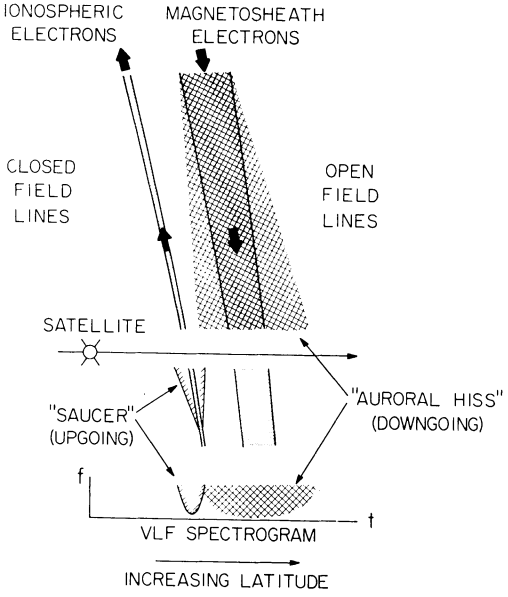

Fig. 8. Illustrative model showing the generation regions of VLF hiss and saucer emissions and their relationship to precipitating magnetosheath electrons and upgoing low-energy ionospheric electrons.

suggestive that this may also be the altitude where the primary auroral acceleration process occurs.

Acknowledgments. This research was supported in part by the National Aeronautics and Space Administration under contracts NAS5-10625, NAS1-8141, NAS1-8144(f), NAS1-8150(f), and grant NGL-16-001-043(7), and by the Office of Naval Research under contract N00014-68-A-0196-0003.

* * *

The Editor thanks F. V. Coroniti and T. R. Hartz for their assistance in evaluating this paper.

REFERENCES

Cauffman, D. P., and D. A. Gurnett, Double-probe measurements of convection electric fields with the Injun 5 satellite, *J. Geophys. Res., 76,* 6014, 1971.

Cloutier, P. A., H. R. Anderson, R. J. Park, R. R. Vondrak, R. J. Spiger, and B. R. Sandel, Detection of geomagnetically aligned currents associated with an auroral arc, *J. Geophys. Res., 75,* 2595, 1970.

Eather, R. H., and S. B. Mende, Airborne observations of auroral precipitation patterns, *J. Geophys. Res., 7,* 1746, 1971.

Ellis, G. R. A., Low frequency electromagnetic radiation associated with magnetic disturbances, *Planetary Space Sci., 1,* 253, 1959.

Frank, L. A., Plasma in the earth's polar magnetosphere, *J. Geophys. Res., 76,* 5202, 1971*a*.

Frank, L. A., Comments on a proposed magnetospheric model, *J. Geophys. Res., 76,* 2512, 1971*b*.

Frank, L. A., and K. L. Ackerson, Observations of charged particles precipitated into the auroral zone, *J. Geophys. Res., 76,* 3612, 1971.

Frank, L. A., and D. A. Gurnett, On the distribution of plasmas and electric fields over the auroral zones and polar caps, *J. Geophys. Res., 76,* 6829, 1971.

Gurnett, D. A., A satellite study of VLF hiss, *J. Geophys. Res., 71,* 5599, 1966.

Gurnett, D. A., G. W. Pfeiffer, R. R. Anderson, S. R. Mosier, and D. P. Cauffman, Initial observations of VLF electric and magnetic fields with the Injun 5 satellite, *J. Geophys. Res., 74,* 4631, 1969.

Gurnett, D. A., S. R. Mosier, and R. R. Anderderson, Color spectrograms of very-low-frequency Poynting flux data, *J. Geophys. Res., 76,* 3022, 1971.

Hartz, T. R., Particle precipitation patterns, in *The Radiating Atmosphere, 1970,* edited by B. M. McCormac, p. 222, Van Nostrand Reinhold, New York, 1971.

Heikkila, W. J., and J. D. Winningham, Penetration of magnetosheath plasma to low altitudes through the dayside magnetospheric cusps, *J. Geophys. Res., 76,* 883, 1971.

Helliwell, R. A., *Whistlers and Related Ionospheric Phenomena,* p. 288, Stanford University Press, Palo Alto, Calif. 1965.

Johnson, R. G., and R. D. Sharp, Satellite measurements on auroral particle fluxes, in *Atmospheric Emissions,* edited by B. M. McCormac and A. Omholt, p. 219, Van Nostrand Reinhold, New York, 1969.

Jørgensen, T. S., Interpretation of auroral hiss measured on Ogo 2 and at Byrd station in terms of incoherent Cerenkov radiation, *J. Geophys. Res., 73,* 1055, 1968.

Kindel, J. M., and C. F. Kennel, Topside current instabilities, *J. Geophys. Res., 76,* 3055, 1971.

Laaspere, T., W. C. Johnson, and L. C. Semprebon, Observations of auroral hiss, LHR noise, and other phenomena in the frequency range 20 Hz to 540 kHz on Ogo 6, *J. Geophys. Res., 76,* 4477, 1971.

McEwen, D. J., and R. E. Barrington, Some characteristics of the lower hybrid resonance noise bands observed by the Alouette 1 satellite, *Can. J. Phys., 45,* 13, 1967.

Mosier, S. R., and D. A. Gurnett, VLF measurements of the Poynting flux along the geomagnetic field with the Injun 5 satellite, *J. Geophys. Res., 74,* 5675, 1969.

Mosier, S. R., and D. A. Gurnett, Theory of the Injun 5 very-low-frequency Poynting flux measurements, *J. Geophys. Res., 76,* 972, 1971.

(Received June 1, 1971;
accepted September 20, 1971.)